ELSEVIER

Journal of Quantitative Spectroscopy & Radiative Transfer 98 (2006) 189–201

Journal of Quantitative Spectroscopy & Radiative Transfer

www.elsevier.com/locate/jqsrt

Correlative studies in optical reflectance measurements of cerebral blood oxygenation

Siew Kan Wan, Zhixiong Guo*

Department of Mechanical and Aerospace Engineering, Rutgers, The State University of New Jersey, 98 Brett Road, Piscataway, NJ 08854, USA

Received 1 December 2004; accepted 10 May 2005

Abstract

A numerical study is made of correlation development for measuring cerebral blood oxygen saturation (StO) noninvasively using optical reflectance ratio of dual wavelengths. The Monte Carlo (MC) method was used for simulating reflectance measurements in a model neck tissue, where the cerebral blood oxygenation was monitored through the blood flows in the common carotid artery (CCA) and jugular vein. Reflectance ratios between two wavelengths at 633 and 800 nm were obtained under different blood vessel conditions. The results revealed a quantifiable correlation between the reflectance ratio and the cerebral StO level. Correlations for each of the blood vessel parameters such as the location, size, and hemoglobin concentration of the CCA or jugular vein (JV) were developed.

Keywords: Reflectance ratio of dual wavelengths; Radiative transfer; Cerebral blood oxygenation; Correlations; MC simulation; Noninvasive diagnosis

1. Introduction

Noninvasive and continuous monitoring of blood oxygenation state in the human brain is of paramount importance in the frontier of human space exploration. Astronauts in space will typically experience headward fluid shift: a condition where fluid in tissue and blood begins to

*Corresponding author. Tel.: 1 732 4452024; fax: 1 732 445 3124.
E-mail address: guo@jove.rutgers.edu (Z. Guo).

0022-4073/$ - see front matter © 2005 Elsevier Ltd. All rights reserved.
doi:10.1016/j.jqsrt.2005.05.083

pool in the upper body due to the microgravity environment. As a result, nerve cells detect this phenomenon as abnormal and begin to reduce body fluid through urination. Within three to five days in space, total water content in body stabilizes at about 2–4% below the normal level and plasma volume decreases about 22% [1]. Such acute changes result in a series of compensatory mechanisms and affect the physiology of the blood. They disrupt astronaut's physical and mental ability to perform critical tasks efficiently. Therefore, an ideal noninvasive tool for continuously monitoring blood oxygenation in human brain needs to be developed.

Apart from space use, a noninvasively and continuously monitoring system is also beneficial to patients who suffer from brain trauma. There are basically two phases in brain damage. The primary injuries consist of direct breakdown of fiber tracts, nerve cells, and blood vessels that a patient encounters during an accident. However, most fatalities in brain trauma patients are caused by the emergence of the secondary phase [2], which could occur within minutes or days later after the accident. Damages in the secondary phase are due to the disorientation of body's systemic functions that may include cerebral ischemia, hyperemia, formation of free radicals and excitotoxins, and intercellular accumulation of calcium [3]. These physiological changes would disrupt the normal oxygen consumption in brain tissues, which is clearly reflected in the blood oxygenation changes in the common carotid artery (CCA) and jugular vein (JV) [4]. With proper and regular monitoring of patients' brain functions, the mortality rate could certainly be reduced significantly.

There are a few methods currently available to scan for the extent of brain damages before and after surgeries. The most common ones are the magnetic resonance imaging (MRI), computed tomography (CT), intracranial pressure (ICP), and jugular venous catheter monitoring system [5]. The later two methods are invasive. Presently, the MRI and X-ray based CT are the two most effective approaches in diagnosing and determining the extent of head injuries for surgeons to plan for operations. However, these two methods cannot be used as the continuous post surgery monitoring system due to the associated health risk, radiation overdose, large facility and considerable expense. For example, the effective radiation dose from a single CT scan is estimated to be two millisieverts or equivalent to an average of eight months of background radiation exposure [6]. The ICP monitoring uses a catheter inserted into the head with a pressure-sensing device, which may cause additional brain damage because a tiny hole has to be drilled through the patient's skull. The jugular venuous catheter monitoring system uses optical technology to measure the absorption spectrum of blood in the bulb of internal JV to determine its oxygen saturation state. On the other hand, inserting catheter inside an artery is impossible due to the high systolic pressure in the artery. Knowing that the CCA/JV supplies/drains most of the cerebral blood with minimal contamination from extracerebral sources [7], brain's oxygen metabolic demand can be estimated based on the blood flow rate and the StO difference between CCA and internal JV [4].

The use of optical technology in biomedical field has been studied extensively over the past few decades not only because it is harmless to human, but it also holds the key potential to a variety of functional imaging that can be related to blood absorption spectroscopic measurements [4,8]. However, characterizing optical measurement through noninvasive means to produce useful information has been known to be a formidable task due to the highly scattering nature of light in biological tissue. Pulse oximetry [9] has been proposed for in vivo measurement of blood oxygenation change. In this principle, the transmission intensity of two different

wavelength laser-emitting diodes (LED) across a finger or ear lobe are measured. Due to the difference of absorption spectra for oxy-hemoglobin and deoxy-hemoglobin, any given blood oxygenation state would yield a unique intensity ratio between the two wavelengths. The simple Beer–Lambert absorption rule is used for calibration and the StO state in the finger can be determined through the detected light intensity ratio. Nonetheless, there exist several limitations associated with the current device. One of the major limitations comes from the fact that the blood perfusion state in the finger and ear lobe is very low. In addition to that, unaccounted absorption in individual skin pigmentation in the less volume finger or ear lobe tissue could render the method less sensitive and less accurate to minute blood oxygenation changes [10].

Currently a few researchers [8,11,12] are developing noninvasive cerebral hemodynamic measurement tools using two or more near-infrared (NIR) wavelengths. The NIR lasers are incident and detected at multiple positions around the head to resolve for local blood oxygenation based on calibrated absorption intensity. Those methods could provide low spatial and temporal cerebral StO states. But they have to go through a time-consuming inverse modeling process, and thus, are not an ideal tool for continuous monitoring. If we can find correlations between the cerebral StO states and the measurements, however, the incontinuously monitoring problem due to time-consuming data processing can be solved.

In this paper, numerical studies are conducted to investigate the correlation between cerebral StO state and optical reflectance ratio of dual wavelengths. CCA and JV blood vessels are considered because they supply and extract most of the blood to and from our head, and can be utilized for characterizing the cerebral metabolic rate of oxygen. In addition, they are close to the neck skin surface and large in size. These facilitate the optical reflectance measurement. The reflected signals will be simulated using a Monte Carlo (MC) program in a two-dimensional (2-D) multilayered tissue model that consists of a skin layer, an embedded blood vessel and two surrounding muscle tissue layers. Two wavelengths, at 633 and 800 nm, respectively, will be applied and the reflectance ratio between them will be related to the blood's oxygen saturation level. The present investigation focuses on the effects of the CCA or JV blood vessel's location, size, and hemoglobin concentration on the reflectance ratio. These parameters vary from one individual to another. Therefore, they have to be taken into account for accurate determination of StO level in the CCA and JV. The selections of incident light wavelength and detector position will also be discussed.

2. The models

2.1. Measurement and tissue model

The reflectance measurement for a neck tissue model is shown in Fig. 1. A continuous-wave (CW) laser beam from a LED was incident perpendicularly to the neck skin surface at the center location and the reflected signals were detected from a parallel detector. The distance between the beam incident spot and the detector is L. The LED was tunable and operated at 633 and 800 nm wavelength in turn. The reflected signal strength for each incident wavelength was measured and divided by the incident signal strength to obtain the reflectance. The reflectance ratio is obtained by dividing the reflectance detected at 633 nm by the reflectance detected at 800 nm.

The neck tissue model consists of a rectangular tissue with four separate tissue layers. The dimension of the tissue model is $H \times W$. The first layer is the skin of neck and its thickness is fixed as $H_s = 1.5$ mm for all the simulations. The second and fourth layers represent the neck muscle tissue while the third layer represents the CCA or internal JV blood vessel. The thickness of the second and fourth layers depends on the specific depth and size of the CCA/JV being investigated. The thickness (diameter) of the CCA or JV blood vessel, H_v, varies from 3 to 4 mm and the depth D, measured from the top skin surface to the middle of the blood vessel varies from 4 to 7 mm.

The skin layer considered is a combination of epidermis and partial dermis layer that does not contain blood capillaries. Therefore, the skin's optical properties are assumed to be constant throughout the simulations conducted. The skin's scattering and absorption coefficients at 633 and 800 nm are adopted from Simpson's paper [13] and listed in Table 1.

Unlike the skin, the muscle tissue contains blood capillaries that affect the overall absorption coefficient as different blood oxygen saturation (StO) levels are considered in the study. The average volume fraction of blood capillaries over the muscle tissue is about 1%. Therefore, the change in absorption coefficient of the muscle tissue is calculated based on 1% of the change

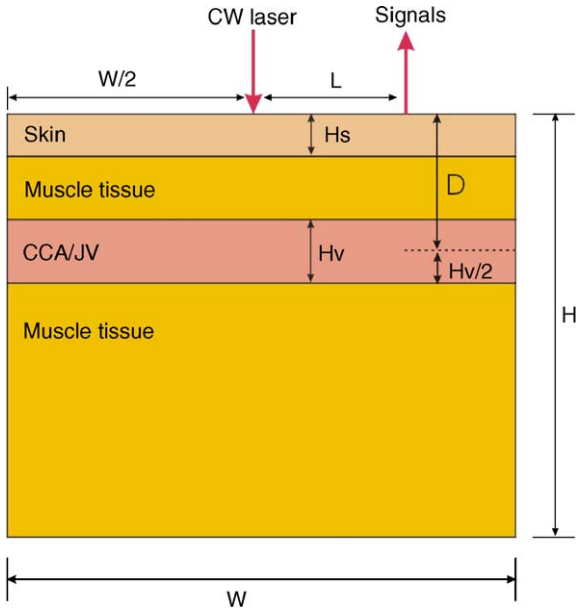

Fig. 1. Sketch of reflectance measurements in a neck-tissue model.

Table 1
The reduced scattering and absorption coefficients of the skin

Wavelength (nm)	μ_s' (mm^{-1})	μ_a(mm^{-1})
633	2.75	0.0345
800	1.91	0.0128

Table 2
The reduced scattering and absorption coefficients of the muscle tissue at various blood StO levels

StO (%)	633 nm		800 nm	
	μ_s' (mm^{-1})	μ_a(mm^{-1})	μ_s' (mm^{-1})	μ_a(mm^{-1})
100	0.908	0.017000	0.778	0.0120000
90		0.017126		0.0119996
80		0.017253		0.0119993
70		0.017379		0.0119990
60		0.017506		0.0119987
50		0.017632		0.0119984

found in whole blood at different blood oxygenation state relative to 100% StO as follows:

$$\mu_{\text{tissue,StO}=X\%} = \mu_{\text{tissue,StO}=100\%} \times \left[1 + 0.01 \times \frac{\mu_{\text{blood,StO}=X\%} - \mu_{\text{blood,StO}=100\%}}{\mu_{\text{blood,StO}=100\%}}\right]. \quad (1)$$

We assumed that the StO state only affects the absorption coefficient, thus leaving the reduced scattering coefficient constant. The tissue's scattering and absorption coefficients at 633 and 800 nm assuming 100% StO are adopted from Doornbos's study [14] and presented in Table 2. The absorption coefficients were based on an average hemoglobin concentration of 15 g/dL [15]. This average value is used in the present studies if the hemoglobin concentration is not particularly indicated. In each of the characteristic studies in the next section, reflectance results were simulated for blood oxygenation state ranging from 50% to 100%—indicating the normal lower and higher limits of vein and artery oxygen saturation states.

The absorption coefficient of the CCA or internal JV is calculated according to the following expression:

$$\mu_a(\text{mm}^{-1}) = 2.303E\ (\text{mm}^{-1}/\text{M}) \times H_b(\text{g/L})/64,500\ (\text{Da}), \quad (2)$$

where E is the combined extinction coefficient of oxy-hemoglobin and deoxy-hemoglobin and is a function of wavelength and StO. The values of the extinction coefficients were obtained from Prahl's website [15]. H_b represents the hemoglobin concentration in the blood and is set to 15 g/dL. It should be noted that H_b will become a variable in the study that characterizes the influence of hemoglobin concentration on the reflectance. The value 64,500 Da refers to the molecular weight of hemoglobin.

2.2. Monte Carlo model

The optical reflectance measurement is simulated using the MC method. Guo et al. [16] developed the basic of the MC model for simulating optical reflectance and transmittance when laser was incident to highly scattering turbid media like biological tissue. Guo et al. [17] further considered the handling of Fresnel reflection boundaries and validated the MC model with experimental measurements. Wan et al. [18] extended the MC method to incorporate an

inhomogeneity inside a homogeneous tissue model. The present MC simulations basically adopted the program code developed from those studies. Modifications to the code are made with respect to the CW nature of the incident laser and the multilayered structure of the tissue model. The CW nature of the laser can be easily considered by dropping the time history in photon bundle tracing. The treatment of multilayered tissue is more complicated and described below.

Biological tissue is generally highly scattering against red and NIR light. The scattering path length is governed by a probability distribution, which will defer according to the extinction coefficient of the layer in which the photon bundle lies; and is given by

$$l = -\frac{1}{\mu_e}\ln(\Re), \tag{3}$$

where μ_e represents the extinction coefficient of a particular tissue layer in which the photon bundle starts to travel and $\Re$ the random number generated by a computer. In the event where a photon bundle traverses from one layer to the next layer, the optical length $\mu_e l$ will be replaced by $\mu_{e1}l_1 + \mu_{e2}l_2$. The subscripts 1 and 2 denote corresponding properties before and after the interface of the two adjacent layers. Since both μ_e and μ_{e1} correspond to the same extinction coefficient of medium before the scattering event, $\mu_{e1} = \mu_e$, and the remainder path length is calculated based on the conservation of optical length given below

$$l_2 = \mu_{e1}(l - l_1)/\mu_{e2}. \tag{4}$$

Similarly, we can treat the case when a photon bundle penetrates three or four tissue layers.

Because of the big difference of refractive indices between the tissue and air, Fresnel reflection must be considered at skin–air interface [19]. All other three sides of the tissue model are actually internal boundaries. Therefore, the reflection at these three sides is set to match the distribution similar to multiple internal scattering events. That is a diffuse reflection with a reflectance of 0.50. We do not consider the difference of reflective indices between different tissue layers because this difference could be slight. Thus, internal reflection at the interfaces of two adjacent tissue layers is neglected. We assume a constant refractive index of 1.40 for the whole tissue.

The statistical errors in MC simulations can be reduced via increasing the number of photon bundles in tracing. On the other hand, the increment of photon bundles will increase the CPU time needed for calculation. There should be a compromise of the trade-off between CPU time and simulation accuracy. The MC method used has been well justified in our previous publications [16–18]. However, it is not needless to verify its accuracy against the photon bundle number selection for the present simulation model. Fig. 2 shows the comparison of the MC simulation results for three different photon bundle numbers. The tissue model is as follows: $H = 20$, $W = 30$, $H_v = 3$, $L = 7$, and $D = 5$ mm. It is seen that the predicted reflectance ratios from the three photon bundle numbers match with each other very well. As compared with the result from the emission of a large photon bundle number (10^9), the average fluctuations of the results for the 10^7 and 10^8 photon bundles are 0.331% and 0.216%, respectively. Thus, a total of 10^8 photon bundles were generally used for all the simulations below. Each simulation took about one hour to produce the results in a DELL PC with one 2-GHz Pentium 4 CPU.

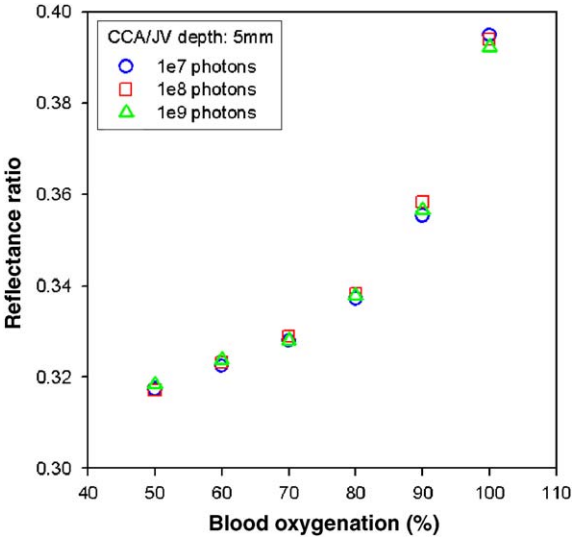

Fig. 2. Effect of the photon bundle number in the MC model on the simulated reflectance ratio.

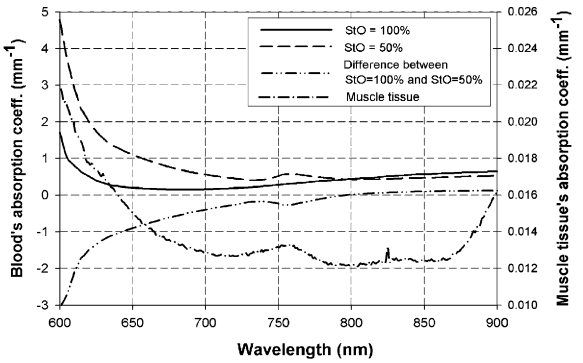

Fig. 3. The absorption spectra of the blood at two limit StO levels and of the muscle tissue.

2.3. Wavelength selection

The objective of this study is to characterize the change of reflectance ratio between two incident radiation wavelengths vs. the blood oxygenation state of the CCA/JV. Therefore, it is necessary to maximize the change in reflectance ratio for a given unit change in blood oxygenation to increase the sensitivity and accuracy. There are several factors to be considered. First of all, the absorption coefficient in the muscle tissue has to be lower than that in the artery/vein for the two operating wavelengths in order to maximize the dependence of signal change vs. the blood oxygenation state inside the artery/vein. Fig. 3 shows the absorption coefficient spectra of blood ($H_b = 15\,g/dL$) with 50% and 100% blood oxygenation, respectively, as well as the difference between them and the absorption spectrum of muscle tissue. The reference wavelength is chosen at

800 nm which is known as the isobestic point, because it is immune to the change in blood oxygenation. Since, all optical properties are constant at 800 nm, signal uncertainty due to motion artifact can easily be detected and compensated. From Fig. 3, the sensitivity of the reflectance ratio between the dual wavelengths would increase if the second wavelength could operate at the red region of visible spectrum or lower. However, it is clear that using wavelength in the vicinity of 600 nm is not practical because the total attenuation in blood will be so high that few of the light photons will be able to travel back to the detector to relay the information gathered from the CCA or internal JV. By testing several simulations with wavelength varied from 600 to 650 nm, we selected the second wavelength at 633 nm.

2.4. Detector position

The detector location also plays an important role in maximizing the reflectance signal's sensitivity. In general, the intensity of the reflected light decreases exponentially as the detector recedes from the laser source [20,21]. A detector located in a close vicinity to the laser source would produce strong signal intensities. The drawback is that the signal would be less sensitive to the change of the optical properties at the CCA and JV. On the contrary, a detector located very far from the laser source would produce very weak signals because of the high density of tissue. In order to determine an ideal location compromising the sensitivity and signal strength, we ran several simulations by varying the location of detector from $L = 3$ to 9 mm. The results of the reflectance ratios for different detector locations are presented in Table 3. The percentage change in reflectance ratio between 50% and 100% blood oxygenation levels as well as the average reflectance are also included. It is clearly seen that the tendency found in percentage change is the opposite of average reflectance. Considering the laser source power range of 1–100 mW and sensitivity of detectors to the order of nanowatts, we have chosen a distance of $L = 7$ mm between the laser and detector as the ideal location; and this value was used in all the simulations if it were not specified otherwise.

2.5. Dimension of the tissue model

The dimension of the tissue model needs to be justified. The height H and width W of the model tissue should be selected such that the simulation results are not influenced by the tissue dimension. Fig. 4 demonstrates the effect of tissue dimension on the simulated reflectance results.

Table 3
Comparison of reflectance ratio, signals' percentage change and average reflectance for various distances between the detector and laser source

Detector distance L (mm)	Reflectance ratio R_{rd} (50% StO)	Reflectance ratio R_{ru} (100% StO)	Percentage change (%)	Average reflectance
3	0.580	0.591	2.76	0.030453
5	0.414	0.444	7.25	0.004401
7	0.349	0.399	14.33	0.001421
9	0.305	0.369	20.10	0.000475

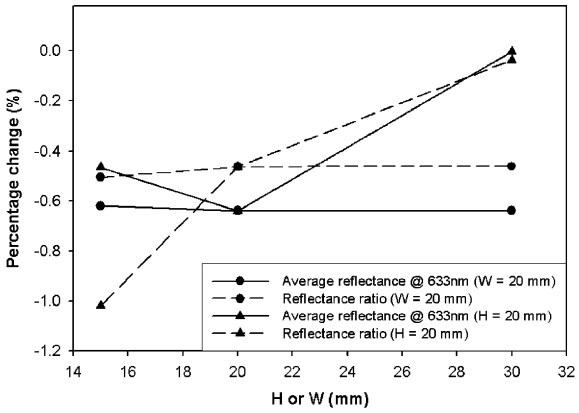

Fig. 4. Effect of the tissue dimension on the simulated results.

The results from a large tissue model of 40×40 mm were selected as the reference values. The relative percentage changes of the relevant parameters over their respective reference value are displayed. It is seen that a tissue with dimension of $H = 20$ and $W = 30$ mm is adequate and this dimension is selected for all the simulations below. In general, $H_v = 3$ and $D = 6$ mm, if they are not specifically mentioned.

3. Results and discussion

There are three characterizations of CCA/JV blood oxygenation measurement being investigated in the following. They are the characterization of reflectance ratio with the changes in the CCA/JV depth D, diameter H_v, and hemoglobin concentration C_{Hb}. The influences of these three parameters are studied because they affect the profile of the reflectance ratio vs. the blood StO level.

Depending on the placement of the laser-detector system and individual patients, the depth of the CCA or JV can vary. The variation could affect the overall magnitude of the reflectance ratio for each blood oxygenation states, but might retain the general pattern. Therefore, accurate determination of blood oxygenation state requires the knowledge of the CCA/JV depth and signal profiling. The determination of blood vessel's depth can be achieved with the aid of ultrasound scan. The profiles of the reflectance ratio vs. the StO for various CCA/JV depths are displayed in Fig. 5. The discrete symbol results are from MC simulation, while the solid-line results are from correlation (6) we find later in this section. Since the absorption coefficient is lower at 100% StO than at 50% StO for 633 nm wavelength, the magnitude of reflectance ratio increases with blood oxygenation. The difference in reflectance ratio between the CCA/JV blood vessel located at 4 and 7 mm deep is much larger at 50% StO level than at 100% StO level. This phenomenon can be explained from the absorption point of view. As mentioned earlier, the higher the contrast between the absorption coefficients of the blood vessel and background tissue, the higher the sensitivity in detected signals. As such, this observation is consistent with the higher absorption found at lower StO level.

Another main feature that has to be characterized is the variation of CCA/JV diameter. There are two types of variation. The first one is the diameter variation due to periodic pressure fluctuation of heartbeat. Normal peak pressure would result in the expansion of elastic artery/vein in the range of several tenth of micrometer [22,23]. We conducted several simulations to investigate the influence of the minute diameter change and found that it affects no more than one percent of the blood oxygenation change from the average diameter's blood oxygenation. Therefore, we have omitted the contribution of this factor due to its insignificance as compared to other factors in the present studies. The second type is the variation of diameter due to the deviation along the artery/vein and among different individuals. This type of variation strongly affects the magnitude of the reflectance ratio. Fig. 6 shows the reflectance ratio and blood oxygenation relationship for normal artery/vein disparity ranging from 3 to 4 mm. The depth of the blood vessel is fixed at 6 mm during the simulations. The larger is the blood vessel size, the smaller is the reflectance ratio. This is because a larger blood vessel volume increases the overall absorption of the tissue. As a result, the reflectance reduces. For any given StO state, the difference in reflectance ratio between the two extreme diameters in Fig. 6 is smaller than that

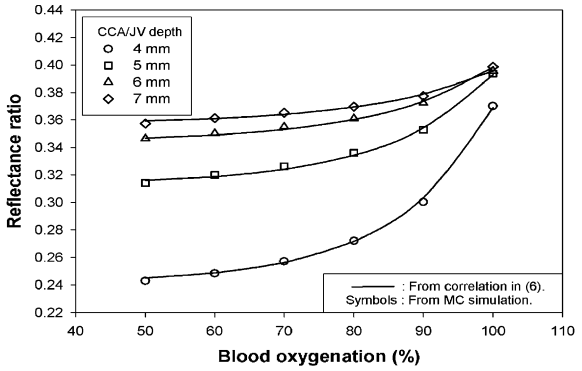

Fig. 5. Reflectance ratio vs. blood oxygenation for various blood vessel depths.

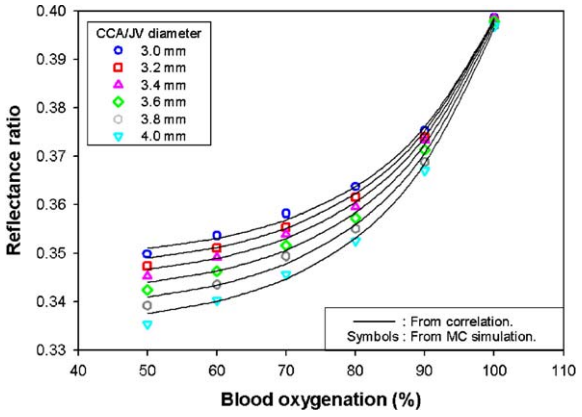

Fig. 6. Reflectance ratio vs. blood oxygenation for different blood vessel diameters.

between the two limit blood vessel depth in Fig. 5. This suggests that the reflectance ratio is more sensitive to artery's/vein's depth—more specifically, the distance from the skin to the CCA/JV blood vessel. The high absorption in the finite artery/vein layer permits only a small percentage of photon bundles to successfully penetrate and return with the information beyond the artery/vein layer. This is why the depth dimension in the tissue model has little effect on the measurement results as shown in Fig. 4.

Besides the physical variation in CCA and JV, the concentration of hemoglobin in blood also affects the reflectance ratio strongly. The absorption chromophores of oxy- and deoxy-hemoglobin in the visible spectrum are significant and have to be taken into account when determining the blood oxygenation level. Fig. 7 shows the profiles of reflectance ratio vs. blood oxygenation for hemoglobin concentration ranging from 11 to 19 g/dL. The results are for the case where CCA/JV depth and diameter equal to 6 and 3 mm, respectively. The absorption coefficient in the blood is proportional to the concentration of hemoglobin. Consequently, the percentage change in absorption coefficient per unit change in hemoglobin concentration is higher for 100% StO than for 50% StO due to its lower absolute absorption coefficient (see Fig. 3). That is why the change in the reflectance ratio against the H_b concentration is larger for higher StO levels. This trend is of reverse order as compared to the previous two figures.

The plots found in Figs. 5–7 can be best fitted with exponential functions in the form below:

$$R_r = A + B\exp(\mathrm{StO}/C), \tag{5a}$$

where R_r is the the measured reflectance ratio and A, B and C are three expressions that are functions of the variable—the parameter of interest, either CCA/JV depth D, diameter H_v, or hemoglobin concentration C_{Hb}.

From the results in Figs. 5–7, we figure out proper expressions for A, B, and C as follows:

$$A = ax^2 + bx + c, \quad B = dx + e, \quad C = fx + g, \tag{5b}$$

in which x is the quantity of the parameter of interest. *a, b, c, d, e, f,* and g are constants and can be obtained from the best fitting technique. Since we are interested in noninvasive determination of blood oxygenation state inside the CCA and JV, the relationship in Eq. (5a) can be rearranged

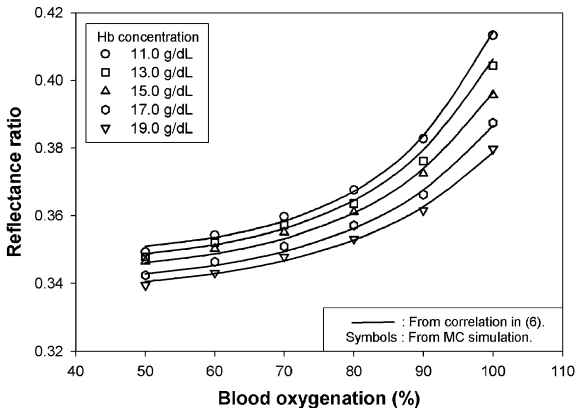

Fig. 7. Reflectance ratio vs. blood oxygenation for different H_b concentrations.

Table 4
The constants for the correlation expressed in Eq. (6)

a	b	c	d	e	f	g
CCA/JV depth correlation: CCA/JV diameter = 3 mm, Hb concentration = 15 g/dL						
−0.0154	0.2075	−0.3397	1.37×10^{-5}	3.01×10^{-5}	1.3174	8.4075
CCA/JV diameter correlation: CCA/JV depth = 6 mm, Hb concentration = 15 g/dL						
−0.0045	0.0176	0.3361	1.47×10^{-5}	9.37×10^{-5}	−0.3268	17.9489
Hb concentration correlation: CCA/JV depth = 6 mm, CCA/JV diameter = 3 mm						
−0.0001	0.0044	0.3042	2.01×10^{-5}	-5.18×10^{-4}	0.4768	11.6925

such that R_r is the measurable quantity. Finally, we obtain the following correlation expression:

$$\mathrm{StO} = (fx + g)\ \ln\{[R_r - (ax^2 + bx + c)]/(dx + e)\}. \tag{6}$$

Since there were three independent parameters, we got three correlations, respectively, for the CCA/JV depth and diameter, and H_b concentration. The values of the constants for the three correlations are listed in Table 4. Statistical analysis revealed that the coefficients of correlations are 0.99562, 0.99017, and 0.996618, respectively, for the CCA/JV depth, diameter, and H_b concentration correlations. The standard deviations for the correlations are calculated to be 0.003728, 0.0002267, and 0.000932, respectively. Thus, the relevance of the correlations is excellent.

4. Conclusions

MC simulations are conducted to determine cerebral blood oxygenation saturation noninvasively using dual wavelength optical reflectance measurement at the CCA and jugular vein. The selections of irradiation wavelength, dimension of model tissue, and detector position are examined. The StO level can be determined through the measurement of the reflectance ratio of the dual wavelengths. However, the determination is not straightforward. The CCA/JV depth, diameter, and H_b concentration are found to affect strongly the values of the reflectance ratio for any given blood StO level. Fortunately, they only affect slightly the general pattern for the profiles of blood StO vs. reflectance ratio. Correlated relationships between the reflectance ratio and the StO are then obtained, respectively, for individual variable parameters of either CCA/JV depth or diameter, or H_b concentration. The values of the constants for the correlations are obtained through the best fitting technique. The relevance of the developed correlations is excellent because the coefficients of the correlations are very close to unity. The significance in finding correlations is that a correlation could be used for determining cerebral blood StO in real time such that continuous monitoring is possible.

Acknowledgment

Grant support from the New Jersey Space Grant Consortium (NJSGC 02-40 and NJSGC 03-44) to this project is gratefully acknowledged.

References

[1] Graham JF. Space exploration from talisman of the past to gateway for the future. http://www.space.edu/projects/book/index.html.

[2] Lewis SB, Myburgh JA, Reilly PL. Detection of cerebral venous desaturation by continuous jugular bulb oximetry following acute neurotrauma. Anaesth Intensive Care 1995;23:307–14.

[3] Sikes PJ, Segal J. Jugular bulb oxygen saturation monitoring for evaluating cerebral ischemia. Crit Care Nurse 1994;17:9–20.

[4] Valadka AB, Furuya Y, Hlatky R, Robertson CS. Global and regional techniques for monitoring cerebral oxidative metabolism after severe traumatic brain injury. Neurosurg Focus 2000;9(5):1–3.

[5] Kristen CK, Laura C. Using jugular venous catheters in patients with traumatic brain injury. Crit Care Nurse 2001;21:16–22.

[6] National Cancer Institute. http://www.cancer.gov/cancertopics/causes/radiation-risks-pediatric-CT.

[7] Eisenhart K. New perspectives in the management of adults with severe head injuries. Crit Care Nurse 1994;17:1–12.

[8] Dunn AK, Devor A, Bolay H, Andermann ML, Moskowitz MA, Dale AM, Boas DA. Simultaneous imaging of total cerebral hemoglobin concentration, oxygenation, and blood flow during functional activation. Opt Lett 2003;28:28–30.

[9] Mihm F, Halperin B. Non-invasive detection of profound arterial desaturation using a pulse oximetry device. Anaesthesiol 1985;62:7.

[10] Huch A, Huch R, Konig V, Neuman MR, Parker D, Yount J, Lubbers D. Limitations of pulse oximetry. Lancet 1988;1:357–8.

[11] Hebden JC, Gibson A, Yusof RM, Everdell N, Hillman E MC, Delpy DT, Arridge SR, Austin T, Meek JH, Swyatt J. Three-dimensional optical tomography of the premature infant brain. Phys Med Biol 2002;47:4155–66.

[12] Cheung C, Culver JP, Yodh AG, Takahashi K, Greenberg JH. In vivo cerebrovascular measurement combining diffuse near-infrared absorption and correlation spectroscopies. Phys Med Biol 2001;46:2053–65.

[13] Simpson CR, Kohl M, Essenpreis M, Cope M. Near infrared optical properties of ex-vivo human skin and subcutaneous tissues measured using the Monte Carlo inversion technique. Phys Med Biol 1998;43:2465–78.

[14] Doornbos RMP, Lang R, Aalders MC, Cross FW, Sterenborg HJCM. The determination of in vivo human tissue optical properties and absolute chromophore concentrations using spatially resolved steady-state diffuse reflectance spectroscopy. Phys Med Biol 1999;44:967–81.

[15] Prahl S. Optical absorption of hemoglobin. http://omlc.ogi.edu/spectra/hemoglobin/.

[16] Guo Z, Kumar S, San KC. Multidimensional Monte Carlo simulation of short-pulse laser transport in scattering media. J Thermophys Heat Tr 2000;14:504–11.

[17] Guo Z, Aber J, Garetz BA, Kumar S. Monte Carlo simulation and experiments of pulsed radiative transfer. JQSRT 2002;73:159–68.

[18] Wan SK, Guo Z, Kumar S, Aber J, Garetz BA. Noninvasive detection of inhomogeneities in a turbid media with time-resolved log-slope analysis. JQSRT 2004;84:493–500.

[19] Bartlett MA, Jiang H. Effect of refractive index on the measurement of optical properties in turbid media. J Opt Soc Am 2001;40:1735–41.

[20] Lin S, Wang L, Jacques SL, Tittel FK. Measurement of tissue optical properties by the use of oblique-incidence optical fiber reflectometry. Appl Opt 1997;36:136–43.

[21] Kienle A, Lilge L, Patterson MS, Hibst R, Steiner R, Wilson BC. Spatially resolved absolute diffuse reflectance measurements for noninvasive determination of the optical scattering and absorption coefficients of biological tissue. Appl Opt 1996;35:2304–14.

[22] Stankus A, Alonderis A. An analysis of the relationship between carotid artery pulsation and heart rate variability. Heart rate variability and cardiovascular pathology. Palanga; 1999, p. 111–33.

[23] Hasegawa H, Kanai H, Hoshimiya N, Chubachi N, Koiwa Y. Noninvasive evaluation of local elastic property of arterial wall using ultrasound. Proceedings of world congress on ultrasound, 2CP23, 1997. pp. 386–7.